Available online at www.sciencedirect.com
ScienceDirect
Ceramics International 38 (2012) 111–117
CERAMICS INTERNATIONAL
www.elsevier.com/locate/ceramint

Investigation of $MoSi_2$ melt infiltrated RSiC and its oxidation behavior

Wenming Guo, Hanning Xiao *, Pengzhao Gao, Wen Xie, Qing Li, Jilin Hu

College of Materials Science and Engineering, Hunan University, Changsha 410082, China

Received 8 February 2011; received in revised form 20 March 2011; accepted 29 April 2011
Available online 25th June 2011

Abstract

Melt infiltration process was employed to fill molten $MoSi_2$ into the pores of recrystallized silicon carbide (RSiC) to improve the oxidation resistance of RSiC, and an almost fully dense RSiC–$MoSi_2$ composite with the microstructure of two-phase interpenetrated network was obtained. The phase compositions of the composites are mainly SiC and $MoSi_2$, including a small amount of $Mo_{4.8}Si_3C_{0.6}$ and Mo_5Si_3. The flexural strength of the composites at room temperature was 11–32% higher than that of as-received RSiC. The cyclic oxidation tests at 1500 °C indicated that both the RSiC–$MoSi_2$ composites and RSiC exhibited a parabolic oxidation behavior, and the corresponding parabolic rate constants of the composites were almost an order of magnitude lower than those of RSiC, resulting in a great improvement of oxidation resistance of RSiC–$MoSi_2$.

Keywords: Recrystallized silicon carbide; RSiC–$MoSi_2$ composite; Melt infiltration; Oxidation resistance

1. Introduction

Recrystallized silicon carbide (RSiC) is generally prepared by the evaporation of very fine SiC particles onto the necks between the large particles at temperature up to 2300 °C. Because there are few impurities in the grain-boundary of RSiC, it maintains excellent creep resistance and high strength at elevated temperatures. RSiC has been receiving attentions as a material for load-bearing parts at high temperature [1], especially in air at 1400–1650 °C. In addition, RSiC is used as thermal exchanger and diesel particulate filter for its high thermal conductivity and relatively low coefficient of thermal expansion (CTE) [2–4].

The consolidation of RSiC does not exhibit any shrinkage during firing because of the evaporation–condensation process, resulting in the porous microstructure of RSiC. Despite the excellent oxidation resistance of SiC, the structure with interconnected pores may be severely detrimental to the properties of RSiC, such as cracking originated from the large pores for the inner oxidation [5]. The weakened oxidation resistance is detrimental to the service life of RSiC. Various techniques, such as applying a dense coating onto the surface of RSiC, are employed to prevent the oxidation of RSiC at high temperatures.

The main purpose of this study is to obtain a dense composite by filling up the pores of RSiC through the melt infiltration process to decrease the inner oxidation so as to improve the oxidation resistance of RSiC. For the application of RSiC at high temperatures under oxidizing conditions, the melting point of infiltrator should be between the ultimate use temperature (~1650 °C) and the consolidation temperature (~2400 °C) of RSiC, and the infiltrator should have satisfactory wettability with RSiC and excellent oxidation resistance. $MoSi_2$ seems to be selectable for infiltration because it is a very attractive intermetallic compound with a high melting point of ~2020 °C which has outstanding oxidation resistance [6]. $MoSi_2$ has a ductile-brittle transition temperature in the vicinity of 1000 °C. It is thermodynamically stable with a wide variety of potential ceramic reinforcements for composites, including SiC, Si_3N_4, Al_2O_3, and TiB_2 [7–10]. Melt infiltration process has been investigated by many researchers utilizing either molten $MoSi_2$ or molten $MoSi_2$ alloyed with other silicides or carbides to infiltrate or reactively infiltrate porous performs of reaction bonded SiC, SiC compacts and carbon [6,11–13]. Lim et al. [6] infiltrated a porous reaction bonded bulk SiC with $MoSi_2$ melts after removal of free silicon, leading to a crack-free composite with high flexural strength that was retained even up to the temperature of 1500 °C and contained significant reaction zone. Esfehanian et al. [13,14] described the

* Corresponding author. Tel.: +86 731 88822269; fax: +86 731 88823554.
E-mail address: hnxiao@hnu.cn (H. Xiao).

0272-8842/$36.00
doi:10.1016/j.ceramint.2011.04.138

development of carbon–silicide–carbide composites free of residual silicon through infiltrating C_f/C preforms and C_f-felts by an alloyed melt, and elaborated an effective infiltration method. Moreover the microstructure and high-temperature mechanical properties of those composites were evaluated.

This work is focused on the fabrication and microstructure of the RSiC–$MoSi_2$ composite and the influence of $MoSi_2$ on the oxidation resistance of RSiC.

2. Experimental procedure

2.1. Preparation of RSiC

Commercial raw materials consisted of coarse SiC and fine SiC powders with different proportions between 70:30 and 50:50 (coarse SiC: fine SiC in mass ratio) of bimodal distribution (Changle Xinyuan Carborundum Micropowder Co. Ltd., Shandong, China). The particle size of fine SiC powder ranges from 0.2 to 1.1 μm (SiC contents > 98.5%, D_{50} = 0.65 μm), while that for the coarse powder ranges from 48 to 120 μm (SiC contents > 99%, $D_{50} = 95 \pm 5$ μm). To obtain RSiC with different densities, the SiC slurries with different volume fractions of SiC and suitable contents of dispersant and binder were slip-cast in a gypsum mold. The green bodies with the subsequent drying process at 100 °C were heated to firing temperature at 2400 °C with a heating rate of 35 °C/min and dwelling time for 1 h in Ar atmosphere. Recrystallization was conducted in the firing process by the evaporation of fine SiC particles and deposition onto the neck of coarse SiC particles. RSiC samples with three grades of density have been obtained as shown in Table 1, which were named based on their relative density values.

2.2. Preparation of RSiC–$MoSi_2$ composite

The obtained RSiC samples in Section 2.1 were used for infiltration. The $MoSi_2$ powder was employed as the raw material for melt ($MoSi_2$ > 98.5%, D_{50} = 6.09 μm, Zhengzhou Songshan Heating Elements Co. Ltd., Zhengzhou, China). Assuming that the porosity of RSiC can be filled by the molten $MoSi_2$, the cooled RSiC–$MoSi_2$ composites would include about 75, 80, and 85 vol% RSiC based on the porosity of RSiC. The composites were named as 75RSiC–$MoSi_2$, 80RSiC–$MoSi_2$ and 85RSiC–$MoSi_2$.

According to the literature [6], the decomposition of $MoSi_2$ may not occur up to 2050 °C, but will aggravate above 2100 °C. Infiltration experiments were mainly conducted at 2050 °C for 1 h in a graphite crucible for the preparation of RSiC–$MoSi_2$. Moreover, infiltration at 2100 °C was also included for comparison to discuss the influence of temperature on the phase composition of the composites.

Table 1
Densification parameters of the obtained RSiC.

Samples	Density (g/cm^3)	Relative density (%)	Apparent porosity (%)
75RSiC	2.38	74.1	25.7
80RSiC	2.55	79.4	20.5
85RSiC	2.74	85.4	14.4

2.3. Characterization

The density of the samples was measured using the water displacement technique (Archimedes method). The flexural strength was determined by three point bending method in a span of 80 mm at room temperature for the samples with the geometrical size of 10 mm × 10 mm × 120 mm, and a loading rate of 0.5 mm/min.

The phase identification was performed by X-ray diffraction (diffractometer) (XRD, Rigaku D/max2200 VPC) using monochromic Cu Kα radiation of 0.15405 nm operated at 40 kV and 40 mA. The morphology and microstructures of the samples were observed by Environmental scanning electron microscope (ESEM, FEI Quanta 200) equipped with an energy dispersive spectrometer (EDS, EDAX).

2.4. Oxidation resistance measurement

For the oxidation resistance measurement, RSiC and RSiC–$MoSi_2$ samples were cut into 15 mm × 10 mm × 10 mm blocks with the surface polished previously. The 8 h cyclic oxidation tests were carried out at 1500 °C in static air using a $MoSi_2$ heating furnace. The samples were placed in the furnace when the temperature was above 1000 °C to avoid the ''pest'' oxidation of $MoSi_2$ for each cycle. The weight change of the samples before and after the cycle were recorded.

3. Results and discussion

3.1. Phase identification, density and microstructure

Fig. 1 shows the XRD patterns of the 80RSiC–$MoSi_2$ composite. The composites infiltrated at 2050 and 2100 °C contained the same main phases of 6H-SiC and $MoSi_2$, including a little of $Mo_{4.8}Si_3C_{0.6}$ and Mo_5Si_3. The relative content of $Mo_{4.8}Si_3C_{0.6}$ seems to be insignificant with the

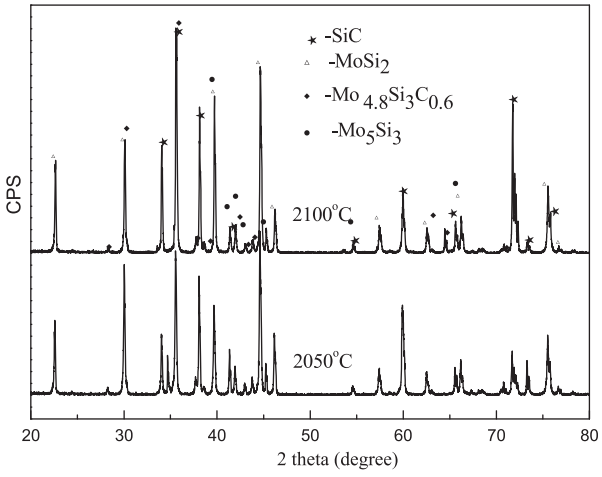

Fig. 1. XRD spectrum of 80RSiC–$MoSi_2$ composite infiltrated at 2050 and 2100 °C.

increase of temperature from the XRD results. It indicates that the melts seem to be stable at the temperature above 2050 °C in the pores of RSiC with only a little amount decomposed, despite the reported sensitive decomposition at this temperature range for $MoSi_2$ [6]. The formation of $Mo_{4.8}Si_3C_{0.6}$ may be related to the decomposition of $MoSi_2$ melt and its reaction with SiC. Due to the similar composition of the composites prepared at 2050 and 2100 °C, only the series at 2050 °C will be discussed in detail next.

The relative densification parameters of RSiC–$MoSi_2$ are shown in Table 2. The density of the composite decreases with

Table 2
Densification parameters of the obtained RSiC–$MoSi_2$ composites.

Samples	Volume of RSiC (%)	Density (g/cm^3)	Apparent porosity (%)
75RSiC–$MoSi_2$	74.1	3.78	3
80RSiC–$MoSi_2$	79.4	3.59	2.52
85RSiC–$MoSi_2$	85.4	3.34	2.99

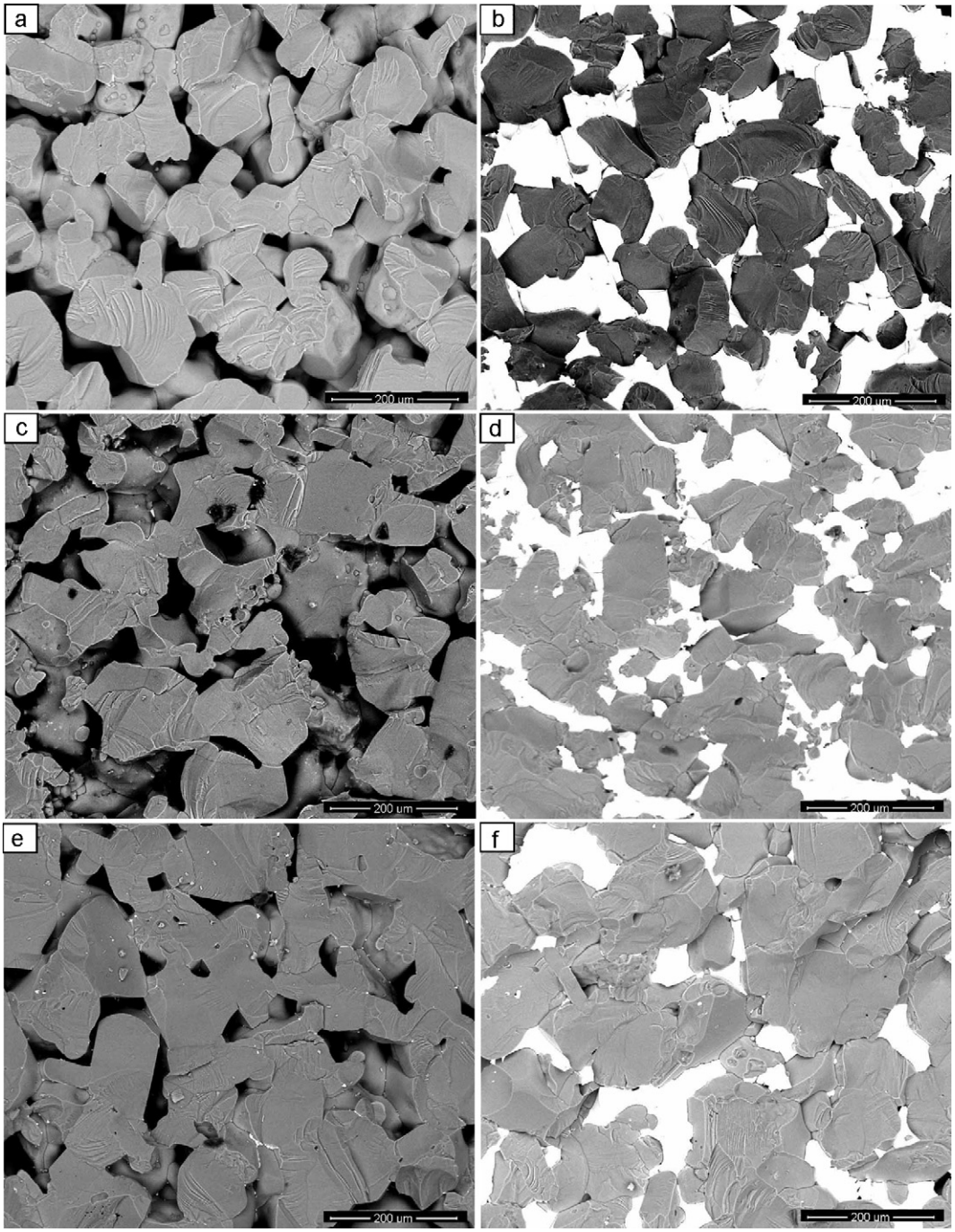

Fig. 2. Microstructure (back-scattered electron image, BEI) of the cross-section of RSiC and RSiC–$MoSi_2$. a, c and e show the microstructure of 75RSiC, 80RSiC and 85RSiC; correspondingly, b, d and f are of 75RSiC–$MoSi_2$, 80RSiC–$MoSi_2$ and 85RSiC–$MoSi_2$.

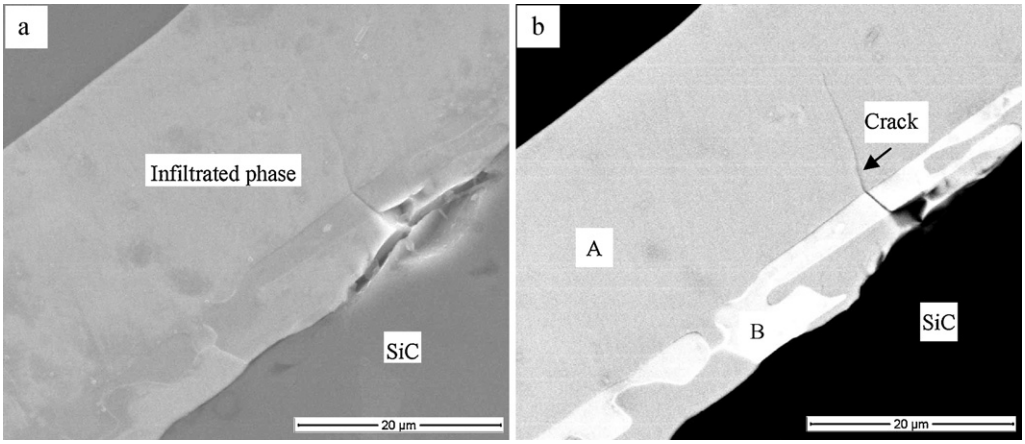

Fig. 3. Microstructure of the polished cross-section of 80RSiC–$MoSi_2$ composite: a, scanning electron micrograph (SEM), and b, BEI of the same area. The corresponding energy dispersive spectrum (EDS) of the point A and B are listed in Table 3.

an increase of RSiC matrix density due to the lower density of SiC (3.21 g/cm^3) than $MoSi_2$ (6.24 g/cm^3), and the apparent porosity of the composites is less than 3%.

The microstructures of RSiC and RSiC–$MoSi_2$ composites are shown in Fig. 2. For the RSiC series, the pores formed surrounding SiC grains are continuous with a net-shape structure which provides the access for $MoSi_2$ melts to infiltrate. Although the pore proportion and its diameter decreased with the increase of the RSiC density (Fig. 2a, c and e), the molten $MoSi_2$ almost completely filled into the pores of RSiC matrix except a few small pores despite the difference of matrix density. Both SiC (gray parts) and $MoSi_2$ (bright parts) seem to be continuous and a RSiC–$MoSi_2$ composite with two-phase interpenetrated network was obtained.

For further observation of the infiltrated phase and its binding with SiC, local microstructures of the polished 80RSiC–$MoSi_2$ composite are shown in Fig. 3. and the corresponding results of EDS analysis displayed in Table 3. The infiltrated phase is wet with SiC (Fig. 3a), and there are two co-existing phases located as A and B in the infiltrated area of Fig. 3b. Combined with the EDS results in Table 3, it is clear that the gray part is $MoSi_2$ and the bright part should be $Mo_{4.8}Si_3C_{0.6}$ or Mo_5Si_3. As elemental carbon cannot be detected by the EDS and the concentration difference of Mo in $Mo_{4.8}Si_3C_{0.6}$ and Mo_5Si_3 is very small, it is hard to distinguish $Mo_{4.8}Si_3C_{0.6}$ and Mo_5Si_3 from BEI observation. In addition, a crack emerged in the infiltrated phase, which originated from the interface of SiC and $MoSi_2$. It is reasonable to consider the crack was caused by the difference of the thermal expansion coefficients between SiC and $MoSi_2$ (SiC: $4.9 \times 10^{-6}\,K^{-1}$ [15], $MoSi_2$: $8.3 \times 10^{-6}\,K^{-1}$ [16]).

Table 3
EDS results of the point A and B in Fig. 3b.

Element	A		B	
	wt%	at%	wt%	at%
Si_K	38.44	68.08	19.21	44.82
Mo_L	61.56	31.92	80.79	55.18

Silicon may evaporate from $MoSi_2$ melt at 2050 °C and above to form a Mo rich phase such as Mo_5Si_3. Furthermore, the Mo_5Si_3 melt may dissolve SiC to form $Mo_{4.8}Si_3C_{0.6}$ and $MoSi_2$ according to the following formula:

$$5MoSi_2 \rightarrow Mo_5Si_3 + 7Si\uparrow \quad (1)$$

$$21SiC + 36Mo_5Si_3 \rightarrow 35Mo_{4.8}Si_3C_{0.6} + 12MoSi_2 \quad (2)$$

3.2. Mechanical properties

Fig. 4 shows the flexural strength of RSiC and RSiC–$MoSi_2$ composites. The strength increase with the increase of relative density of both RSiC and RSiC–$MoSi_2$. The flexural strength of RSiC–$MoSi_2$ composites is only 11–32% higher than that of RSiC samples despite the composites have much higher relative density than RSiC. The small improvement of strength is mostly caused by the unrelieved thermal stresses from the difference of thermal expansion coefficients between SiC and $MoSi_2$.

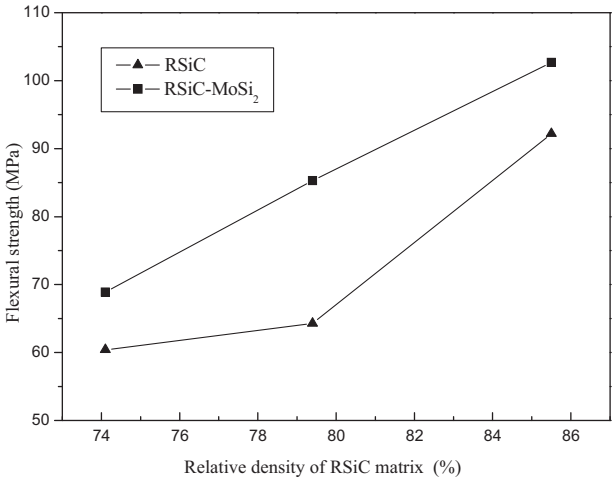

Fig. 4. Flexural strength and porosity of the samples *vs* relative density of RSiC matrix.

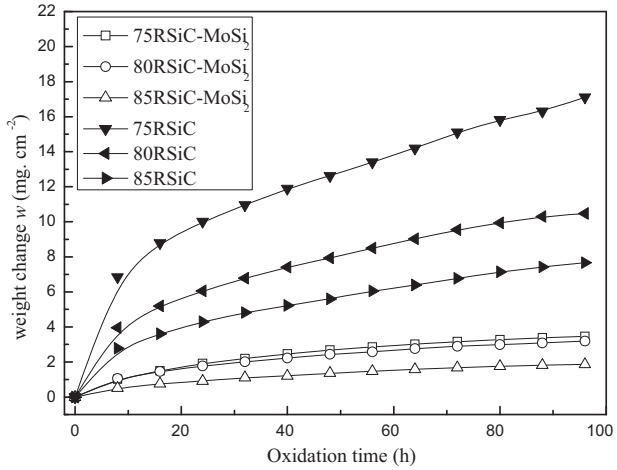

Fig. 5. Weight changes per unit area with the cyclic oxidation time of RSiC and RSiC–$MoSi_2$ composites.

3.3. Oxidation behavior

The weight change versus oxidation time plots at 1500 °C are shown in Fig. 5. The weight gain of RSiC decreases with the increase of RSiC density, owing to the decrease of porosity. The weight gain of RSiC–$MoSi_2$ composites is much lower than that of RSiC. The improvement of oxidation resistance of RSiC–$MoSi_2$ composites is mainly contributed by the large decrease of porosity and the outstanding oxidation resistance of $MoSi_2$.

From the weight gain curves (Fig. 5) and the kinetic analysis in Fig. 6, both the RSiC and RSiC–$MoSi_2$ composites exhibit the parabolic oxidation behavior (R is the correlation coefficient in Fig. 6). The corresponding parabolic rate constants k are listed in Table 4, which were calculated from the formula: $w^2 = kt + b \approx kt$, where w is the weight change (mg/cm^2). The k values of the RSiC series are almost an order of magnitude higher than the value of RSiC–$MoSi_2$ series, which indicates an evident improvement of oxidation resistance of RSiC–$MoSi_2$ composites.

Fig. 7 shows the XRD patterns of the RSiC oxidized at 1500 °C for different times. Before oxidation, only SiC peaks are detected. After 2 h oxidation, the SiO_2 peaks appeared. With the increase of oxidation time, the intensity of SiO_2 peaks increased and that of SiC peaks decreased. Fig. 8 shows the phase evolution of the 80RSiC–$MoSi_2$ composite oxidized at 1500 °C for different times. Similar to the oxidation of RSiC, the SiO_2 peaks appeared after 2 h oxidation, and increased with the oxidation time. However, the peaks of $MoSi_2$ and $Mo_{4.8}Si_3C_{0.6}$ increased first, then decreased after oxidation

Table 4
Kinetic constants k and correlation coefficient R.

Samples	R	k
75RSiC	0.9991	2.71
80RSiC	0.9977	1.09
85RSiC	0.9995	0.58
75RSiC–$MoSi_2$	0.9926	0.13
80RSiC–$MoSi_2$	0.9963	0.10
85RSiC–$MoSi_2$	0.9980	0.04

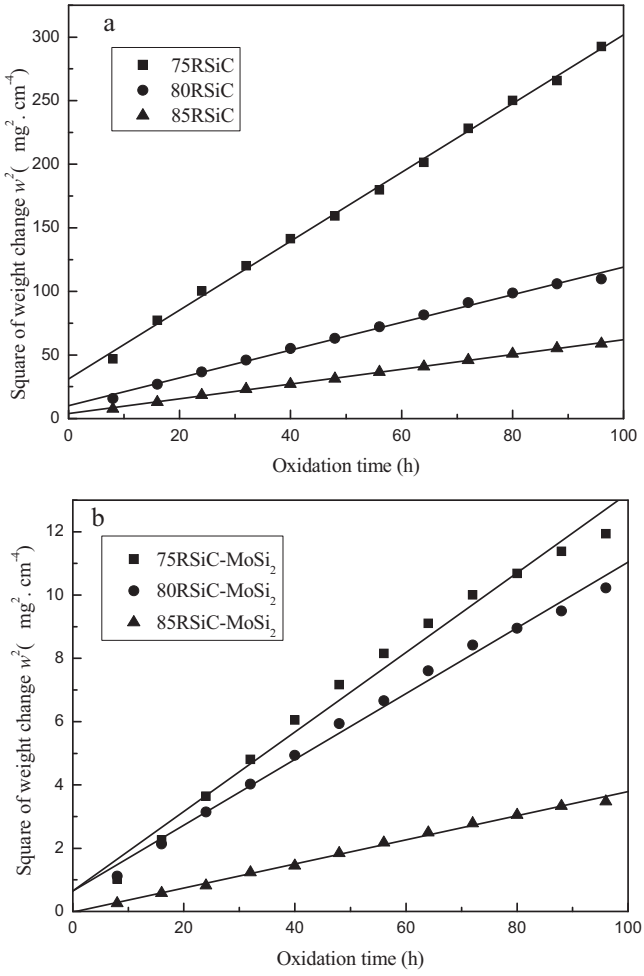

Fig. 6. Relationship between the square of weight change per unit area and the cyclic oxidation time for the kinetic calculation: (a) RSiC; (b) RSiC–$MoSi_2$.

for 40 h. The relatively weak peaks of Mo_5Si_3 emerged when oxidation time was increased to 96 h (Fig. 8b). A possible explanation for the variation of $MoSi_2$ and $Mo_{4.8}Si_3C_{0.6}$ during oxidation in Fig. 8a may be related to the residual Mo_5Si_3 after

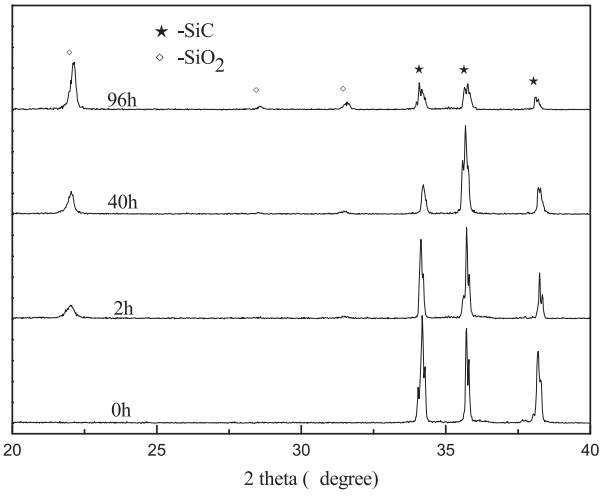

Fig. 7. XRD patterns of the same surface of polished 80RSiC oxidized at 1500 °C for different time.

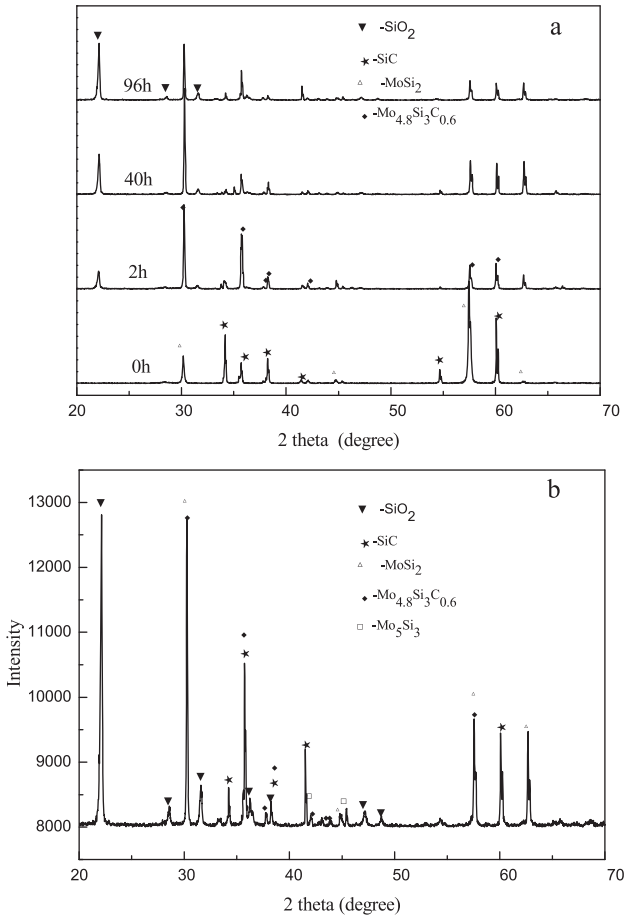

Fig. 8. XRD patterns of the same surface of polished 80RSiC–$MoSi_2$ oxidized at 1500 °C for different time (a) and 96 h (b).

infiltration. The Mo_5Si_3 may react with SiC by diffusion to form $Mo_{4.8}Si_3C_{0.6}$ and $MoSi_2$ expressed in Eq. (2), which was detected at the interfaces between Mo_5Si_3 and SiC by Kaufuman [17]. The transition of residual Mo_5Si_3 resulted in the increase of $MoSi_2$ and $Mo_{4.8}Si_3C_{0.6}$ in the early stages of oxidation. Continued oxidation decreased the two phases; besides the increased SiO_2 layer also decreased the peak intensity of the phases below the SiO_2 layer as the oxidation time increased.

Fig. 9 shows the SEM photographs of the polished cross-section of the 80RSiC oxidized at 1500 °C for 96 h. Fig. 9a indicates the oxidation layer with a thickness of about 3 μm on the surface of RSiC, and Fig. 9b shows the oxidation layer (∼2 μm) of an interior pore. However, the interior part of 80RSiC–$MoSi_2$ composite was rarely oxidized. Oxidation was only observed on the surface and some boundary between SiC and $MoSi_2$, and the thickness of oxidation layer on the surface of RSiC–$MoSi_2$ composite was similar to that of RSiC (also ∼3 μm shown Fig. 10). The much lower weight gain for RSiC–$MoSi_2$ compared to RSiC seems to be contributed by the less surface contacting with oxygen as the pores of RSiC was fully filled by $MoSi_2$.

Compared to the RSiC–$MoSi_2$ composite, the higher weight gain of RSiC is due to the oxidation contributed from both interior pores and exterior surface. Moreover, the interior oxidation may be the destruction source of the RSiC after prolong oxidation. With the increase of the SiO_2 layer and crystallization of amorphous SiO_2, the large difference of the CTE between the SiC matrix and the SiO_2 layer may result in the cracks to appear in the SiO_2 layer during cyclic heating and cooling. The cracks promote the oxidation of SiC under the SiO_2 layer and the cracks will result in the destruction of RSiC when they grow into the SiC matrix. For the RSiC–$MoSi_2$ composite, the interior pores have been filled by $MoSi_2$ melt, resulting in the evident improvement of oxidation resistance and prolonged service life of the composite.

After oxidation at 1500 °C for 96 h, the XRD results indicate a new phase of Mo_5Si_3. The oxidation of $MoSi_2$ is usually considered as selective oxidation of silicon by the following equation:

$$5MoSi_2 + 7O_2 \rightarrow Mo_5Si_3 + 7SiO_2 \quad (3)$$

Generally, a Mo_5Si_3 transition layer will be observed under the surface SiO_2 layer after long time oxidation in single crystal $MoSi_2$. However, this transition layer does not appear in oxidation of $MoSi_2$–SiC composite, despite the fact that new Mo_5Si_3 has been detected by XRD. It is similar to Beatrice's

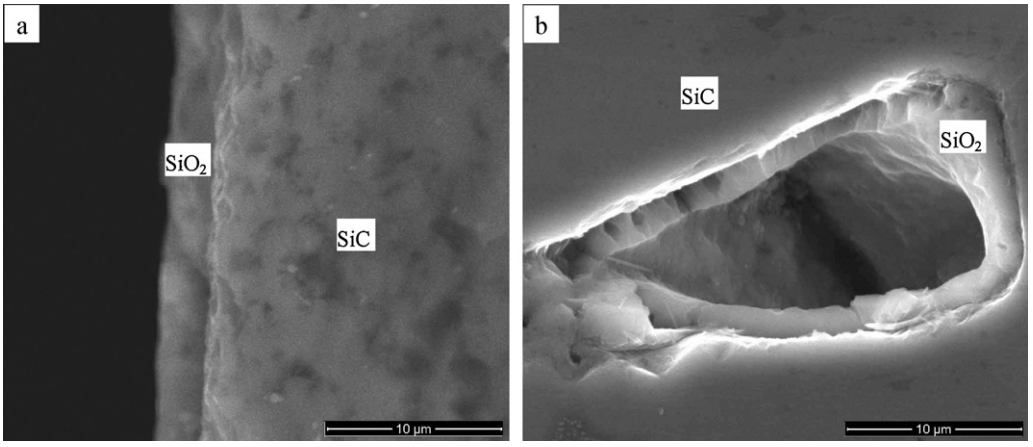

Fig. 9. Microstructure (SEM) of the polished cross-section of 80RSiC after oxidation at 1500 °C for 96 h: (a) exterior, (b) interior of RSiC.

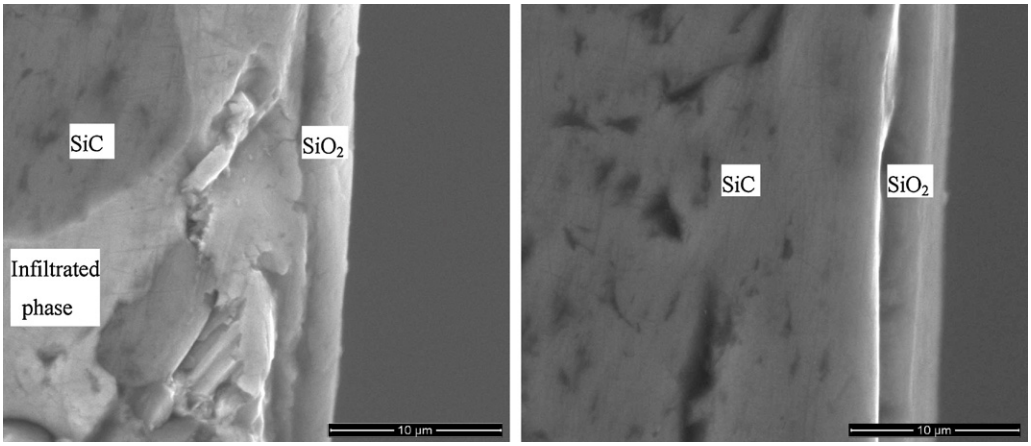

Fig. 10. Microstructure (SEM) of the polished cross-section of 80RSiC–$MoSi_2$ after cyclic oxidation at 1500 °C for 96 h.

study [18] on the oxidation of polycrystalline $MoSi_2$, and the absence of Mo_5Si_3 layer is considered as evidence that the diffusion of Si and/or Mo in $MoSi_2$ is rapid which prevents the necessary concentration build-up to form Mo_5Si_3.

4. Conclusions

Microstructure, phase evolution and oxidation behavior of RSiC–$MoSi_2$ composites containing 15, 20 and 25 vol% $MoSi_2$ were investigated and compared with pure RSiC. The pores of RSiC were fully filled by the $MoSi_2$ melt except only a few small ones, and a structure with two phase interpenetrated network formed. The phase composition of RSiC–$MoSi_2$ composites infiltrated at 2050 and 2100 °C showed little difference, containing mainly SiC and $MoSi_2$, besides a small amount of $Mo_{4.8}Si_3C_{0.6}$ and residual Mo_5Si_3. The formation of $Mo_{4.8}Si_3C_{0.6}$ could be attributed to the decomposition of $MoSi_2$ melt and the dissolution of SiC.

The flexural strength of the composites at room temperature was only 11–32% higher than that of RSiC series despite the near fully dense structure. It is caused by the unrelieved thermal stresses inherent to the composite that resulted from the difference of thermal expansion coefficients between SiC and $MoSi_2$.

The cyclic oxidation test at 1500 °C indicates that the oxidation resistance of the RSiC–$MoSi_2$ was greatly improved compared to that of the RSiC. The corresponding parabolic rate constants of the RSiC–$MoSi_2$ composites are almost an order of magnitude lower than those of the RSiC. The pores filled by $MoSi_2$ mainly contributed to the improvement of the oxidation resistance of the composite as the oxidation only occurred at the surface.

Acknowledgements

The authors thank National Science Foundation of China (Grant No. 50972042) for the grants that support this research.

References

[1] K. Bundschuh, M. Schüze, C. Müller, P. Greil, W. Heider, Selection of materials for use at temperatures above 1500 °C in oxidizing atmospheres, J. Eur. Ceram. Soc. 18 (1998) 2389–2391.

[2] N. Orlovskaja, H. Peterlik, W. Steinkellner, K. Kromp, Prediction of strength of recrystallized silicon carbide from pore size measurement: part 1. The bimodality of the distribution, J. Mater. Sci. 35 (2000) 699–705.

[3] Z.Z. Yi, Z.P. Xie, Y. Huang, J.T. Ma, Y.B. Cheng, Study on gel-casting and properties of recrystallized silicon carbide, Ceram. Int. 28 (2002) 369–376.

[4] C.C. Agraiotis, I. Mavroidis, A.G. Konstandopoulos, B. Hoffschmidt, P. Stobbe, M. l Romerod, V. Fernandez-Queroe, Evaluation of porous silicon carbide monolithic honeycombs as volumetric receivers/collectors of concentrated solar radiation, Sol. Energy Mater. Sol. Cells 91 (2007) 474–488.

[5] A. Sonntag, New R-SiC extends service life in kiln furniture, Am. Ceram. Soc. Bull. 76 (1997) 51–54.

[6] C.B. Lim, T. Yano, T. Iseki, Microstructure and mechanical properties of RB-SiC/$MoSi_2$ composite, J. Mater. Sci. 24 (1989) 4144–4151.

[7] P. Hvizdos, M. Besterci, B. Ballokova, R. Scholl, A. Böhm, Creep behaviour of $MoSi_2$–SiC and $MoSi_2$–HfO_2, Mater. Lett. 51 (2001) 485–489.

[8] C. Suryanarayana, Structure and properties of ultrafine-grained $MoSi_2$ + - Si_3N_4 composites synthesized by mechanical alloying, Mater. Sci. Eng. A 479 (2008) 23–30.

[9] A. Newman, S. Sampath, H. Herman, Processing and properties of $MoSi_2$–SiC and $MoSi_2$–Al_2O_3, Mater. Sci. Eng. A 261 (1999) 252–260.

[10] T. Shu-Qi Guo, T. Nishimura, Y. Mizuguchi, Kagawa, Mechanical properties of hot-pressed ZrB_2–$MoSi_2$–SiC composites, J. Eur. Ceram. Soc. 28 (2008) 1891–1898.

[11] K. shobu, E. Tani, M. Akiyama, T. Watanabe, High-temperature strength of melt-infiltrated SiC–Mo(Al, Si)$_2$ composites, J. Am. Ceram. Soc. 79 (1996) 544–546.

[12] O. Chakrabarti, L. Weisensel, H. Sieber, Reactive melt infiltration processing of biomorphic Si–Mo–C ceramics from wood, J. Am. Ceram. Soc. 88 (2005) 1792–1798.

[13] M. Esfehanian, J. Günster, F. Moztarzadeh, J.G. Heinrich, Development of a high temperature C_f/XSi_2–SiC(X = Mo, Ti) composite via reactive melt infiltration, J. Eur. Ceram. Soc. 27 (2007) 1229–1235.

[14] M. Esfehanian, J. Günster, J.G. Heinrich, J. Horvath, D. Koch, G. Grathwohl, High-temperature mechanical behavior of carbon–silicide–carbide composites developed by alloyed melt infiltration, J. Eur. Ceram. Soc. 28 (2008) 1267–1274.

[15] W.D. Kingery, Introduction to Ceramics, John wiley and Sons, Inc., New York, USA, 1960, p. 473.

[16] T.A. Kircher, E.L. Courtright, Engineering limitations of $MoSi_2$ coatings, Mater. Sci. Eng. A 155 (1992) 67–74.

[17] A. Costa e Silva, M.J. Kaufman, Phase relations in the Mo–Si–C system relevant to the processing of $MoSi_2$–SiC composites, Metall. Mater. Trans. A 25 (1994) 5–15.

[18] P. Beatrice, The High-temperature Oxidation Behavior of $MoSi_2$ and $MoSi_2$-based Composites, PhD Thesis, University of Pennsylvania, USA, 1997, pp. 82–86.